

Article

The Microstructure and Selected Mechanical Properties of Al₂O₃ + 13 wt % TiO₂ Plasma Sprayed Coatings

Monika Michalak , Leszek Łatka * , Paweł Sokołowski , Aneta Niemiec  and Andrzej Ambroziak 

Faculty of Mechanical Engineering, Wrocław University of Science and Technology, Łukasiewicza 5, 50-371 Wrocław, Poland; monika.michalak@pwr.edu.pl (M.M.); pawel.sokolowski@pwr.edu.pl (P.S.); aneta.niemiec@pwr.edu.pl (A.N.); andrzej.ambroziak@pwr.edu.pl (A.A.)

* Correspondence: leszek.latka@pwr.edu.pl

Received: 22 January 2020; Accepted: 11 February 2020; Published: 13 February 2020



Abstract: The Al₂O₃ + TiO₂ coatings are of the interest of surface technology and tribology due to their good wear resistance and enhanced toughness comparing to pure Al₂O₃ coatings. However, the detailed effect of the used feedstock powder, is often neglected. Here, this work focuses on the deposition of Al₂O₃ + 13 wt % TiO₂ coatings by atmospheric plasma spraying (APS) method as well as on their microstructure, phase composition and selected mechanical properties, in the reference to the route of the powder feedstock preparation. The commercial powder Metco 6221 in agglomerated and sintered form was used as a feedstock material during spraying, due to the fact that, so far, sintered or cladded powders are the most studied ones. The 2^k + 1 spray experiment allowed to evaluate the influence of two variables, namely spray distance and torch linear velocity, on the coating microstructure. Afterwards, the coating adhesion was measured by the means of pull-off test. The correlations between Vickers microhardness, fracture toughness (*K_c*) as well as the coating morphology and phase composition were investigated. Finally, the dry sliding wear resistance was studied by using Ball-on-Disc method.

Keywords: plasma spraying; coating; morphology; microstructure; phase composition; roughness; microhardness; fracture toughness; sliding wear resistance

1. Introduction

Plasma spraying is nowadays the primary method used commercially to deposit relatively thick coatings [1,2]. The continuous development of powder materials and spraying equipment, as well as better understanding of the spraying process itself, led to the application of thermal spraying in various fields: aircraft, automotive, power industry, and others [3–7]. One of the most commonly used material combinations for this technique is Al₂O₃ doped with TiO₂ [2,8–11]. The commercial powders of the Al₂O₃–TiO₂ system are usually available with 3 wt %, 13 wt %, and 40 wt % content of TiO₂. In this work, Al₂O₃ + 13 wt % TiO₂ (AT13) coatings deposited by APS were characterized.

It is already well known that AT13 coatings provide high wear resistance and fracture toughness [3,9,12]. Moreover, the use of Al₂O₃ and TiO₂ in one powder particle can provide extended exploitation when compared to pure Al₂O₃. This is due to the fact that the conventional sandblasting applied to the materials with higher melting temperature (such as Al₂O₃) is often not a sufficient procedure to provide durable ceramic–metal bonding. The addition of TiO₂ lowers the melting temperature of such powder and finally results in increased coating adhesion [13].

The motivation of studies on the abovementioned powder stems from the fact that, despite numerous studies and years of industrial applications of such APS coatings, surprisingly there are still

unknown issues [14]. This comes from insufficient attention addressed to the used feedstock powder. Most of the studies present the comparison of coatings made from (i) various nanostructured powders (reconstituted into sprayable micrometric agglomerates) and well-known (ii) Metco 130 powder (in clad form) [2,11,14–18].

Another important issue, is still a lack of understanding about the influence of formation of aluminum titanate (Al_2TiO_5) on the microstructure and mechanical properties of Al_2O_3 -13 wt % TiO_2 coatings [14]. Therefore, in the presented studies, AT13 coatings, derived from agglomerated and sintered powder, were sprayed according to the $2^k + 1$ design of experiment and analyzed in the terms of their morphology, microstructure, phase composition and resulting mechanical and wear properties, including: adhesion, microhardness, fracture toughness (K_{Ic}) and sliding wear resistance. Coatings sprayed from the agglomerated nanopowders, due to their favorable properties, were claimed to found a wide range of application, for example in printing industry and for tribological usage.

2. Materials and Methods

2.1. Materials

A commercially available powder (Metco 6221, Oerlikon, Switzerland) of $\text{Al}_2\text{O}_3 + 13 \text{ wt } \% \text{ TiO}_2$ (AT13) was used as a feedstock material for spraying process. The SEM micrographs (JEOL JSM-6610A, Jeol, Tokyo, Japan) showed that the particles had spherical morphology, as the powder was produced by agglomeration and sintering (Figure 1). Powders consisted of small evenly distributed particles of Al_2O_3 and TiO_2 . The nominal powder particle size range was equal in the range between 15 and 45 μm . The powder particles size was confirmed by laser diffraction granulometry (Horiba Partica LA-950 V2, Horiba Ltd., Kyoto, Japan). The results showed that powder had a volume–surface mean diameter d_{v50} equal to 33.3 μm and was characterized by narrow and monomodal particle size distribution. According to XRD analysis (Bruker AXS, Billerica, MA, USA), powder consisted of α - Al_2O_3 , rutile- TiO_2 , and aluminum titanate Al_2TiO_5 .

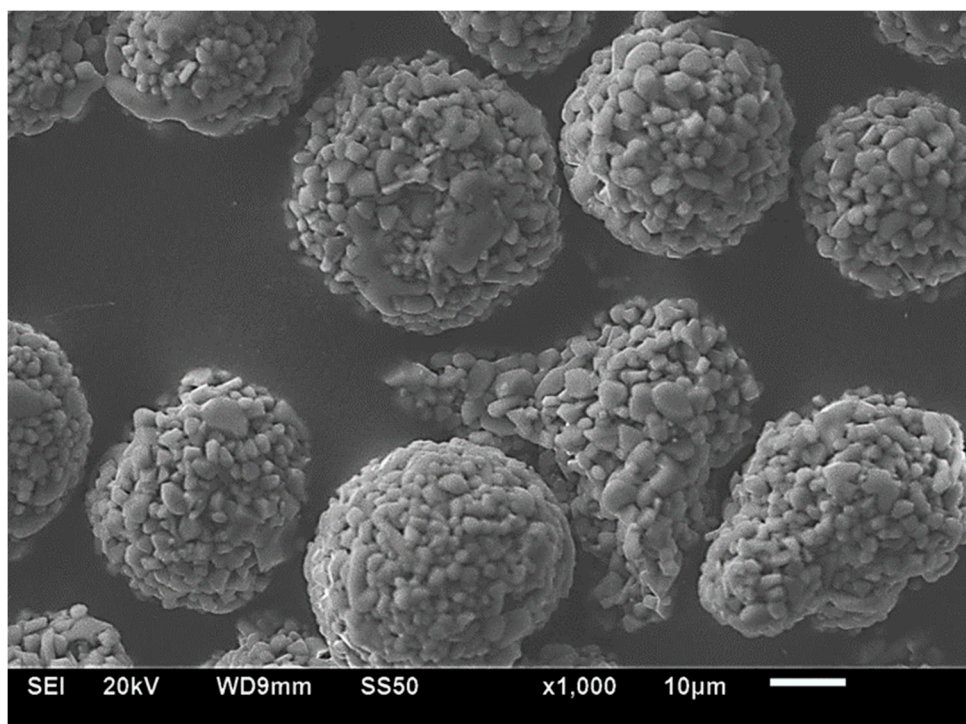


Figure 1. SEM image of $\text{Al}_2\text{O}_3 + 13 \text{ wt } \% \text{ TiO}_2$ powder in the delivery condition.

2.2. Spray Process

Atmospheric plasma spraying (APS) was used to process $\text{Al}_2\text{O}_3 + 13 \text{ wt } \% \text{ TiO}_2$ powders and deposit the coatings. The spray method is already well-established [19]. During spraying the micrometer-sized powders are heated by high-temperature plasma jet and propelled at high velocity to impact the substrate. Splats are created upon the impact of the liquid particle into the substrate and then the coating is formed, layer by layer [20].

Plasma spraying was carried out by the use of one cathode-one anode SG-100 plasma torch (Praxair, Indianapolis, IN, USA). The torch operated at a constant electric power of 35 kW. The working gases composition was Ar + H_2 (45 slpm + 5 slpm) in each case. The plasma torch was fixed to a 6-axis Fanuc 2000 IA robot, whereas the substrates were mounted to the rotating carousel (Figure 2). The 2^k+1 design of experiment (DoE) included two spray variables: spray distance and scan speed of the torch (that means the resultant linear velocity between the torch and rotating substrates). All spray process parameters and sample labels are collected in Table 1. The motivation behind selecting the mentioned variables comes from the literature study, and some of spray parameters have been investigated already, for example plasma power [21].

Table 1. The process parameters and sample labelling.

Sample Code	Spray Distance L, mm	Torch Velocity V, mm/s	Electric Power, kW
AT13-1	80	300	35
AT13-2	80	500	
AT13-3	90	400	
AT13-4	100	300	
AT13-5	100	500	

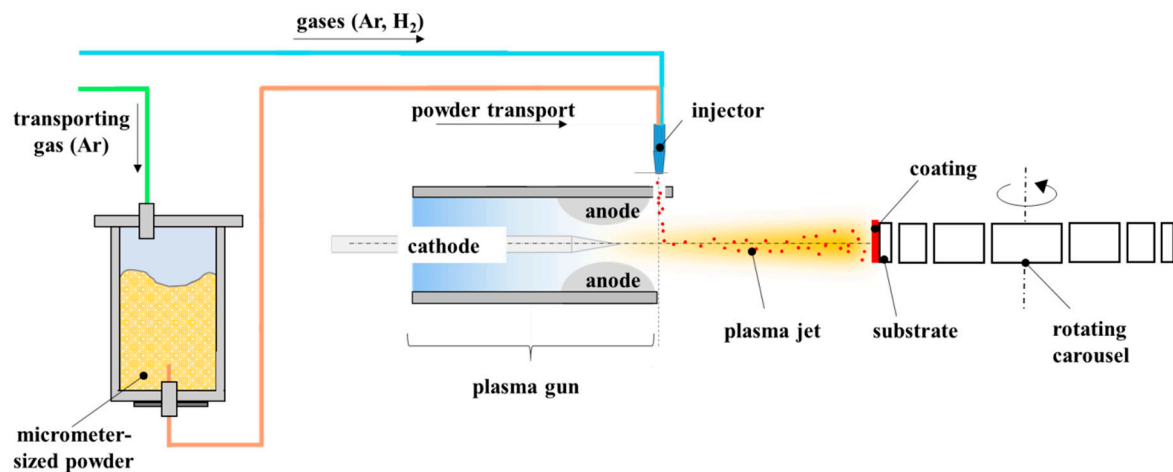


Figure 2. The spray process configuration scheme (inspired by [22] copyright Elsevier 2008).

The feedstock material was injected radially into the plasma jet. The feed rate was about 20 g/min. $\text{Al}_2\text{O}_3 + 13 \text{ wt } \% \text{ TiO}_2$ powders were dried at a temperature of 120 °C for 3 h prior to spraying in order to avoid clogging of powder during feeding. The coatings were sprayed onto 25 mm stainless steel coupons with a thickness of 2 mm. Before spraying, the substrates were sand blasted by using corundum grit (F40 according to FEPA standard) and cleaned with ethanol in an ultrasonic bath.

2.3. Microstructural Characterization

The coatings' free surfaces, as well as their cross-sections, were investigated to observe the microstructural features of deposits. The free surface of coatings was characterized in as-sprayed conditions. The metallographic sampling was performed in order to prepare cross-sections for further

analysis. The samples were sectioned, mounted in an epoxy resin, and then grinded, and mirror-like polished. Afterwards, all samples were gold sputtered to reduce charging effect during scanning electron microscopy investigations. SEM observations were done by Phenom G2 Pro (Phenom-World, Eindhoven, The Netherlands). The main aim was to determine the morphology of coatings, including degree of melting of the particles, appearance of microcracks and voids, etc. The substrate/surface interface was analyzed as well.

Based on SEM micrographs the coating porosity and thickness were evaluated. The micrographs taken at magnification of 1000× were used for the porosity analysis. Then, the Image Analysis (IA) method was applied to count the percentage porosity area of coatings as this method allows counting both open and closed pores. The open source ImageJ software (version 1-50) was used for that purpose and analysis was carried out according to the ASTM E2109-01 Standard [23]. For each sample 20 images were processed to obtain reliable results. The thickness of coatings was measured by using SEM micrographs at 550× magnification. For each sample five measurements were taken at different locations along the coating cross-section. The average values and standard deviations were calculated, for both porosity and thickness.

Phase composition of the initial powders and coatings was determined by powder X-ray diffraction technique (XRD) using D8 Discover diffractometer (Bruker AXS, Karlsruhe, Germany) with CuK α radiation. The measurements were performed in the range $2\theta = 10^\circ \div 80^\circ$, with 0.05° step size and 0.8 s/step counting time.

Finally, the roughness of coatings was measured by stylus profilometer (MarSurf PS 10, Mahr, Germany). The mean values of R_a , R_z , and R_t parameters were calculated. Three measurements on each sample were carried out and average and standard deviation were determined.

2.4. Mechanical Properties

The testing of mechanical properties was started by measurements of coating adhesion. The bond strength was determined by well-known pull-off test and was carried out by dedicated Elcometer 510 tester (Elcometer Instruments, Manchester, UK). A counterpart with the diameter of 10 mm was bonded to the coating using epoxy adhesive Distal Classic (Libella, Warsaw, Poland). Then, continuous pressure of 0.4 MPa/s was applied to the test pin, so the tension at the interface between the coating and counterpart was increased. Once the coating was pulled off, the numerical value of adhesion strength was indicated by the software. After the observations of coating surface and dolly surface, the failure mode was determined. The average value and standard deviation were calculated based on five measurements.

Subsequently, the microhardness of coatings was measured with Vickers penetrator under the load of 1.96 N (HV0.2) using the HV-1000 hardness tester (Sinowon Innovation Metrology, Dongguan, China), according to the standard [24]. For each coating 10 imprints at the cross-section were made and the average values, as well as standard deviations, were calculated.

Fracture toughness (K_C) for the coating–substrate system cannot be easily determined in a similar way as for the bulk materials. A popular approach in surface technology is a method based on measurement of cracks length, which occur in coating after Vickers penetration. The length of the cracks can be related to K_C value according to Palmqvist observation [25]. The further methodology depends on cracks identification and a ratio between l and a parameters (Figure 3). When the l/a ratio is in range from 0.1 to 1.5 then a Niihara model is used to calculate the fracture toughness [26]:

$$K_C = 0.018 \cdot H^{0.6} \cdot E^{0.4} \cdot 2 \cdot a \cdot l^{-0.5} \left[\text{MPa} \cdot \text{m}^{-1/2} \right] \quad (1)$$

where:

H —Vickers hardness (MPa);

E —elastic modulus (MPa);

$2a$ —imprint diagonal (m);

l —average length of cracks (m).

However, when the ratio between l and a is higher than 1.5 then the equation proposed by Anstis et al. should be used [27]:

$$K_C = 0.016 \cdot \left(\frac{E}{H}\right)^{0.5} \cdot \frac{P}{c^{1.5}} \left[MPa \cdot m^{-1/2}\right] \quad (2)$$

where:

$c = a + l$ —total length of crack (m);

P —maximum load of penetrant (N).

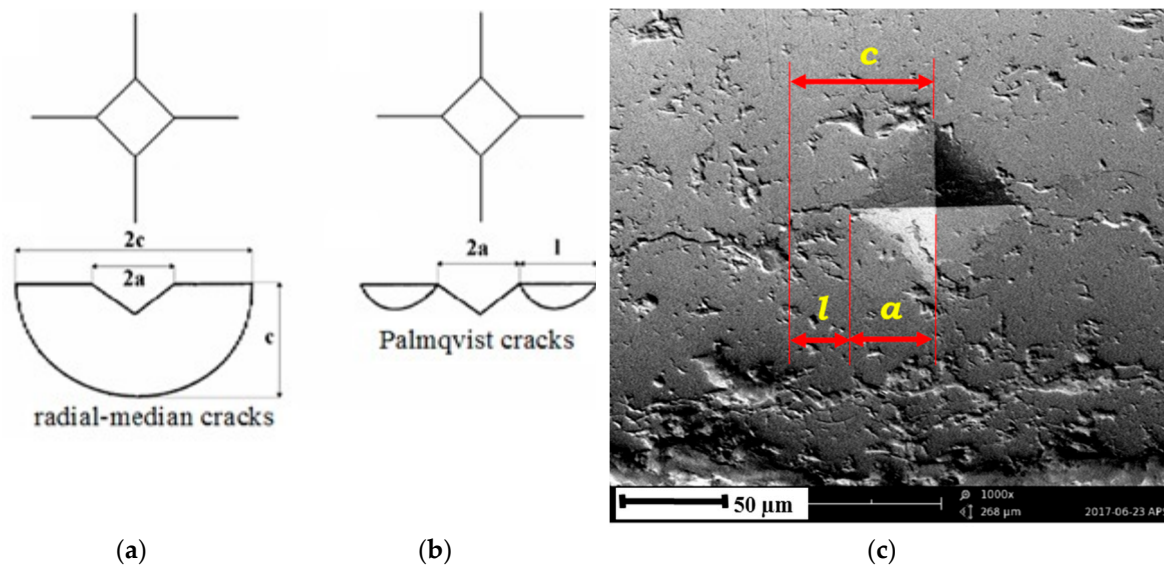


Figure 3. Geometry and vertical section of cracks around Vickers print [28]: (a) radial-median mode, (b) Palmqvist mode, and (c) exemplary crack after Vickers indentation [29].

Ball-on-disc (BoD) dry sliding tests were carried out in rotating unidirectional configuration according to the ASTM G99-17 [30] using T-01 tribometer (Rtec Instruments, San Jose, CA, USA). According to the standard [30], average surface roughness (R_a) of $0.8 \mu\text{m}$ (or lower) is usually recommended. Therefore, coatings were grinded and polished before wear tests and their roughness was controlled after this process.

As a counterpart, 100Cr6 bearing steel balls of 6 mm diameter were used. The tests were performed under ambient conditions, over a distance of 500 m (10,000 cycles). The other parameters used for testing were as follows: relative sliding speed of 0.1 m/s, wear track radius of 6 mm, and normal load of 5 N. Three replicate wear tests were carried out and the average results were reported here.

BoD was conducted with the aim to determine the volume wear rate. The volume wear rate (V_w) was calculated by using as follow equation:

$$V_w = \frac{V}{N \cdot S} \left[\frac{mm^3}{N \cdot m} \right] \quad (3)$$

where:

V —volume (mm^3);

S —sliding distance (m);

N —normal load (N).

The morphology of the wear tracks on the specimens was analyzed using scanning electron microscope (SEM) Phenom G2 Pro.

3. Results and Discussion

3.1. Coating Microstructure

The micrographs of as-produced coatings are collected in Figure 4. It can be seen that the microstructure of coatings was influenced by the spray process parameters (summarized in Figure 5). While the shortest spray distance was used, the coatings were characterized by well-melted lamellas. This can be observed especially on their top surfaces (Figure 4a,c). The increase in the distance between the torch and the substrate caused some of the powder particles to cool down before hitting the substrate. As a result, those coatings (Figure 4e,g,i) were not that homogeneous, with less-flattened deposits, and their microstructure consisted of two regions: fully melted and partially melted areas. Similar results were obtained by Goberman et al. [15]. Furthermore, when comparing coatings sprayed with different torch scan velocities, some differences may be observed as well. Once the lowest torch scan speed was used (300 mm/s), the substrate and coating were highly exposed to heat generated by the plasma torch. As a result, some single inter- and intra-lamellar cracks are visible in those coatings (AT13-1 and AT13-4 presented in Figure 4b,h). On the contrary, once the torch scan speed was increased to 400 or 500 mm/s, the cracking of coatings was almost eliminated.

Dark areas visible in the coatings' cross-section represent pores, voids, and cracks, which are inherent feature of APS coatings [2,9,11]. In all coatings, Al_2O_3 and TiO_2 were evenly distributed [22,30]. It should be noticed that the substrate/coating interface did not reveal any discontinuities—it is well known that addition of TiO_2 to Al_2O_3 improves adhesion between coating and substrate, due to lower melting temperature than of pure Al_2O_3 [9]. In each sample, the rough substrate asperities, being a result of abrasive blasting, were well covered by the $\text{Al}_2\text{O}_3 + 13 \text{ wt } \% \text{ TiO}_2$ splats.

The coatings intended for microstructure investigations were all sprayed with a similar number of spray passes. Coatings of thickness 130–230 μm were obtained. The deposition efficiency was the highest for samples AT13-1 and AT13-4 (equal approximately to 29 $\mu\text{m}/\text{pass}$ and 28 $\mu\text{m}/\text{pass}$), so the lowest torch scan speed and shortest spray distance both had a positive impact on the process effectiveness.

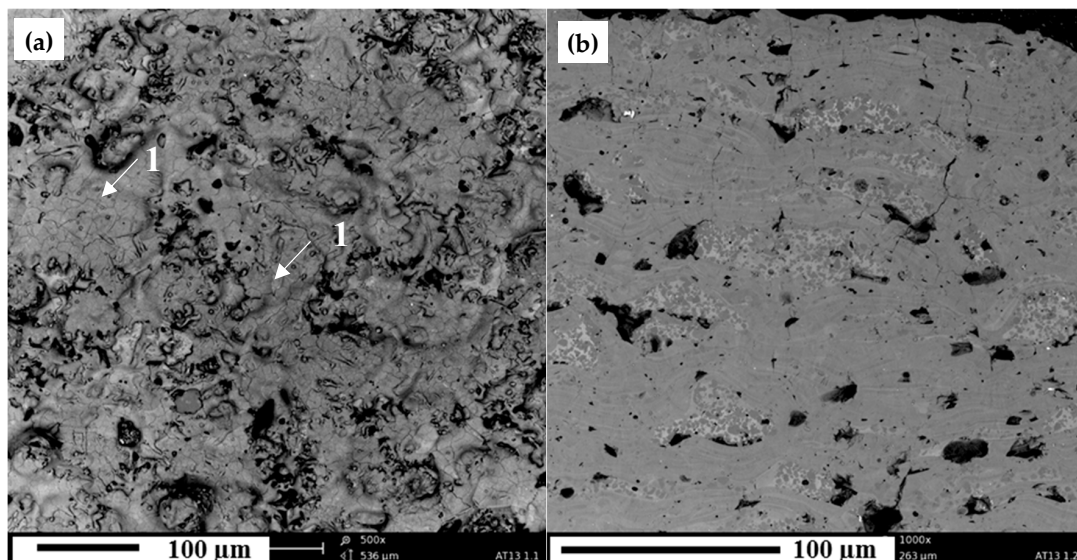


Figure 4. Cont.

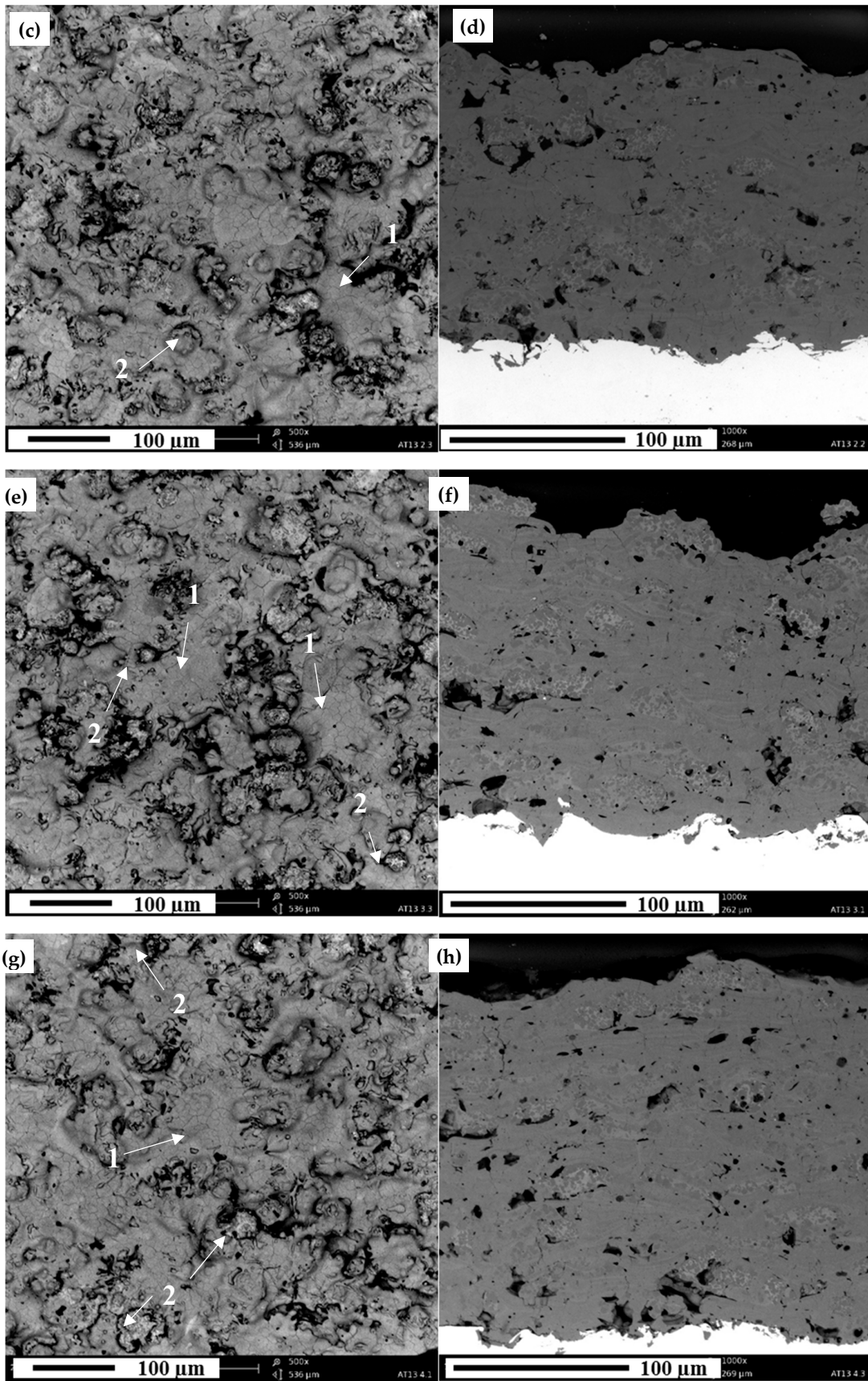


Figure 4. Cont.

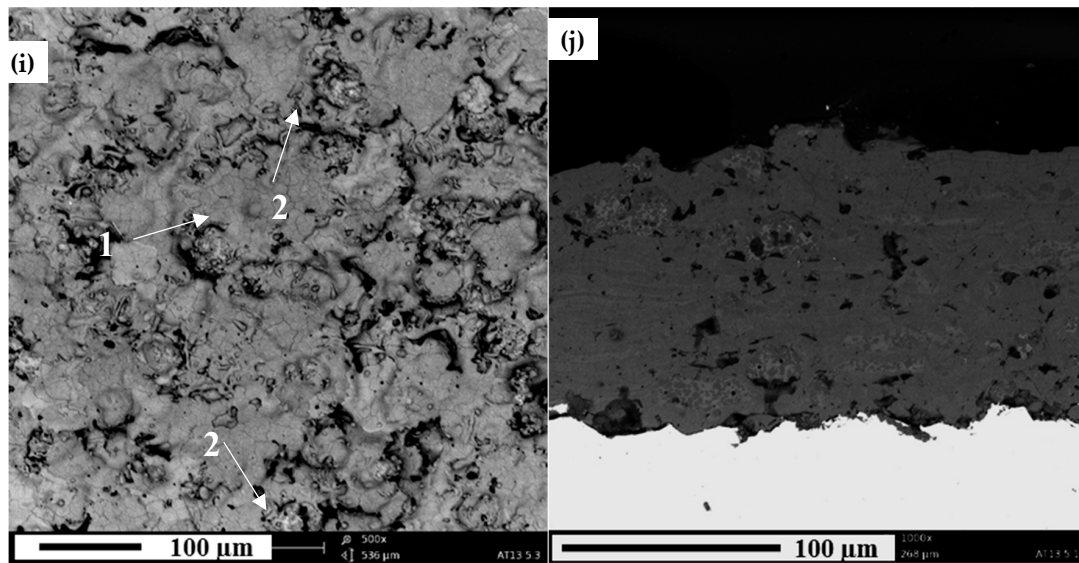


Figure 4. Free surface (left side) and cross sections (right side) of produced coatings: (a,b)—AT13-1 (L = 80 mm; V = 300 mm/s); (c,d)—AT13-2 (L = 80 mm; V = 500 mm/s); (e,f)—AT13-3 (L = 90 mm; V = 400 mm/s); (g,h)—AT13-4 (L = 100 mm; V = 300 mm/s); (i,j)—AT13-5 (L = 100 mm; V = 500 mm/s); 1—fully melted splats, 2—non-melted powder particles.

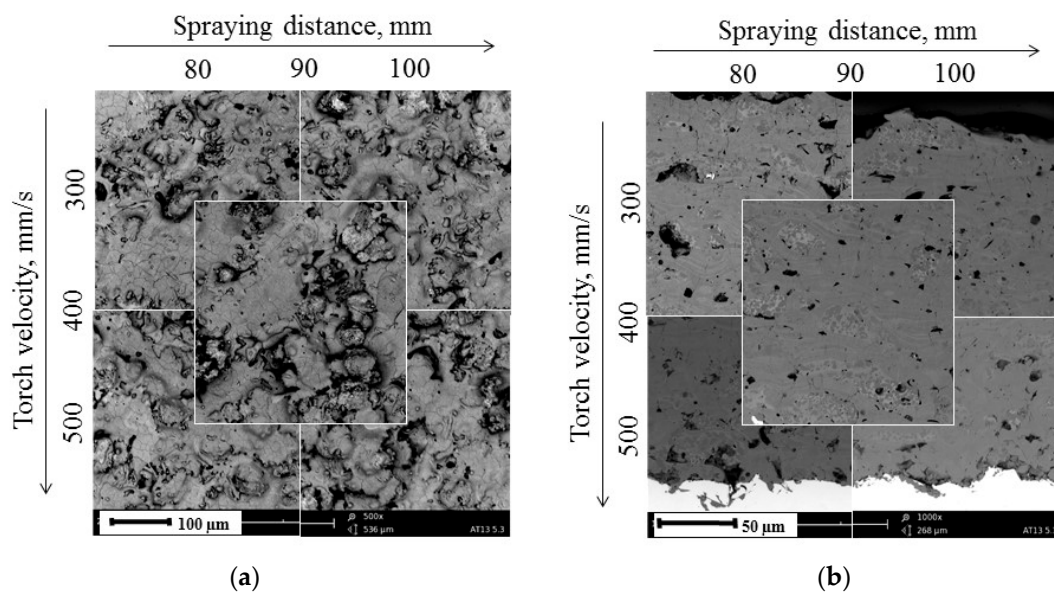


Figure 5. The correlation between spray process parameters and (a) free-surface topography and (b) microstructure of coatings cross sections.

The porosity of the coatings was relatively low, as indicated by the results presented in Figure 6. Similar porosity values were found for all the coatings. They are in the range of results reported in other papers for coatings with similar chemical composition [14,31].

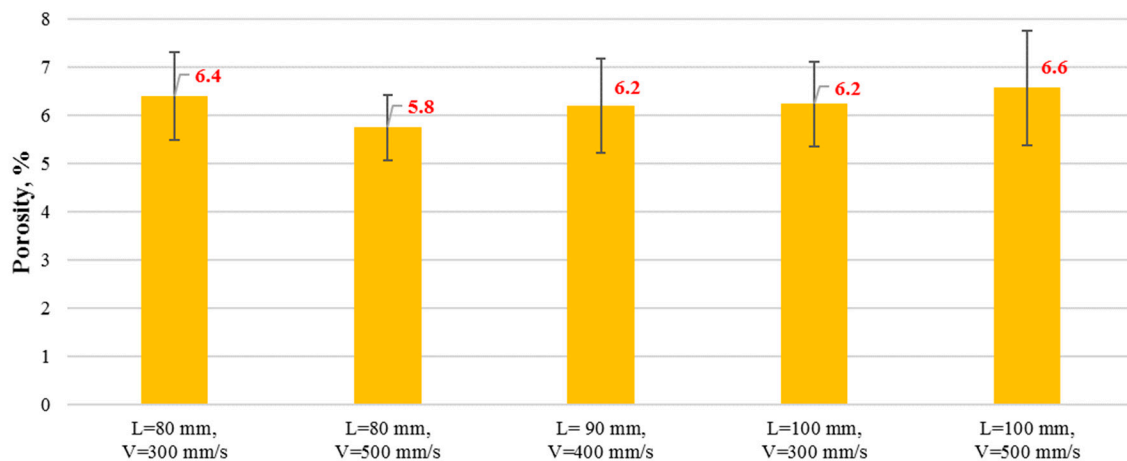


Figure 6. Mean values of coatings porosity.

Finally, the roughness of coatings was investigated. The results are presented in Table 2. It can be seen that all surface topography parameters of the coatings are two to three times greater when comparing them to the substrate material just before spraying. Similar findings have been reported previously [32], so the presented roughness values can be considered as standard for these coatings. The greatest roughness was observed for coatings sprayed at the highest spray distance, which is also usually observed in thermal spraying.

Table 2. Mean values of coatings roughness.

	R_a , μm	R_z , μm	R_t , μm
AT13-1	7.6 ± 0.06	50.1 ± 1.24	61.9 ± 4.20
AT13-2	7.8 ± 0.01	51.3 ± 2.21	62.3 ± 4.49
AT13-3	7.8 ± 0.04	50.5 ± 1.02	61.6 ± 3.54
AT13-4	7.9 ± 0.04	50.2 ± 0.92	61.9 ± 2.39
AT13-5	8.0 ± 0.04	52.7 ± 0.95	62.7 ± 0.29
substrate	3.0 ± 0.01	22.4 ± 0.14	25.8 ± 1.54

Phase composition of deposited coatings is shown in Figure 7. It is clear that during spraying, the thermodynamically stable $\alpha\text{-Al}_2\text{O}_3$ solidified in the metastable $\gamma\text{-Al}_2\text{O}_3$ [14]. These findings were observed in most of the works related to AT13 feedstock powder [2,9,17,32,33]: it is known that $\alpha\text{-Al}_2\text{O}_3$ transforms irreversibly to $\gamma\text{-Al}_2\text{O}_3$ at temperature higher than ~ 1000 °C, due to its preferential nucleation at high cooling rates [11,34–36]. Therefore, the presence of $\alpha\text{-Al}_2\text{O}_3$ peaks indicated that some non-melted powder particles are still present in the deposited coatings. Figure 4 with SEM micrographs confirmed those findings, as discussed above.

When compared the phase composition of all sprayed coatings, it could be observed that the main difference lies in the intensity of aluminum titanate (Al_2TiO_5) peaks, especially for the shortest spray distance (AT13-1). This equimolar compound can be easily synthesized from alumina and titania, but decomposes below 1280 °C into single oxides of Al_2O_3 and TiO_2 [37,38]. As there are significant differences between physical properties of the single Al_2O_3 , TiO_2 , and Al_2TiO_5 , an influence on the coating properties by the existence of Al_2TiO_5 can be expected. However, as shown in recent studies [37,39], the role and effect of Al_2TiO_5 on final coating properties is still not that clear, mainly due to its instability. The relationships between the presence of Al_2TiO_5 and resulting coatings properties is discussed in further sections.

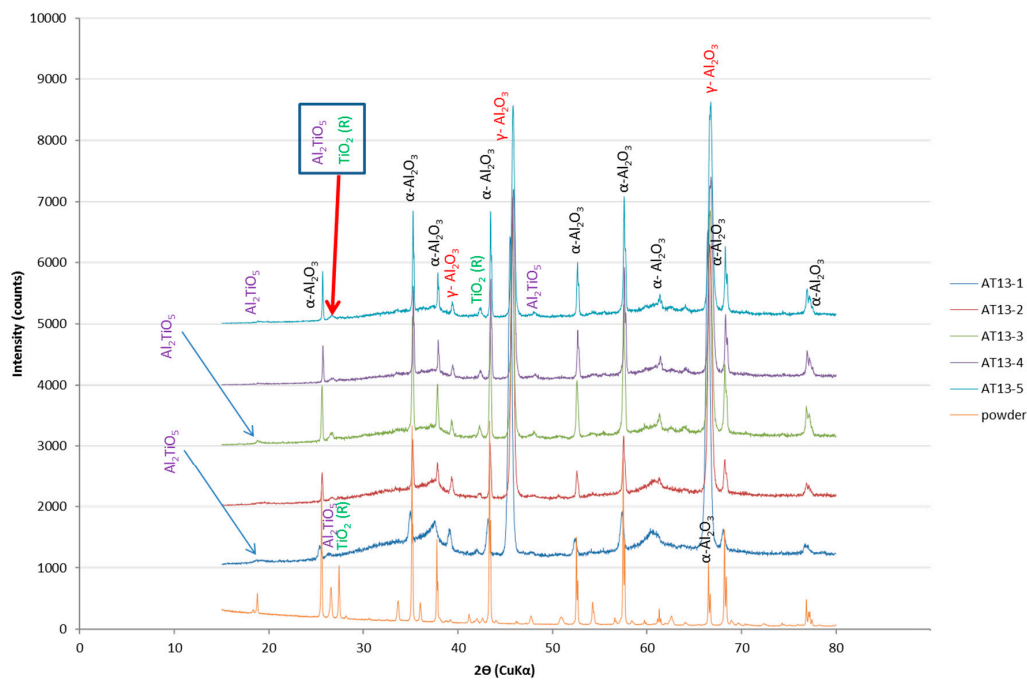


Figure 7. XRD of as-sprayed coatings and as-delivered powder.

3.2. Mechanical Properties

All coatings were investigated in pull-off test in order to determine their adhesion to the substrate. The results of bond strength testing are presented in Figure 8. The mean values of adhesion were ranging from 13.7 ± 2.6 MPa to 16.3 ± 3.5 MPa. In general, the coatings sprayed with shortest spray distance were characterized by higher adherence to the substrate. This can be explained by higher particle velocity influencing the impact momentum. It is believed that the increase in impact momentum improves the flattening of splats and allows better penetration of substrate asperities by deposits. The bond strength of presented coatings was similar to the results reported in literature, and indicated as sufficient for the exploitation [17].

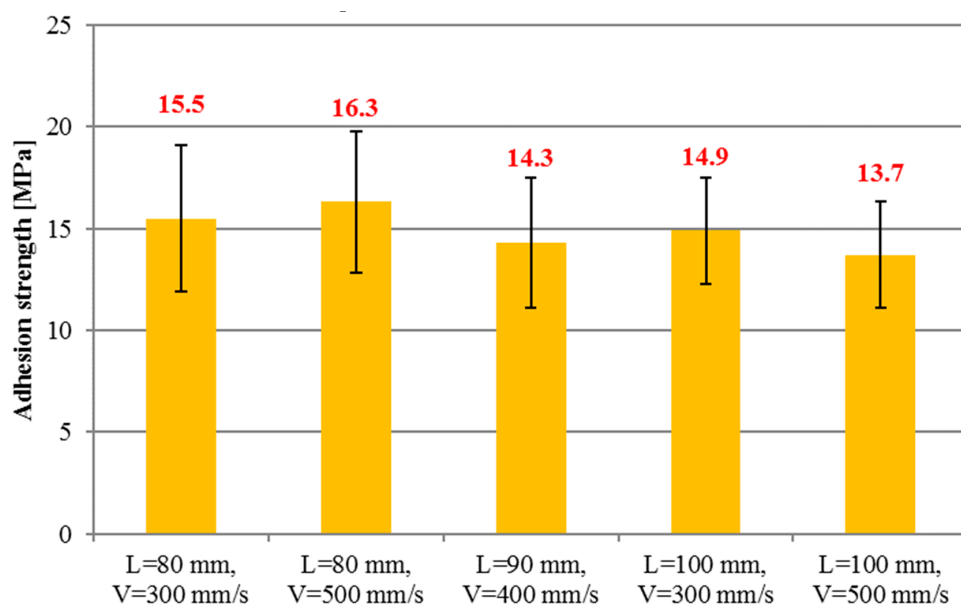


Figure 8. Adhesion strength of AT13 coatings.

Afterwards, the surface of the dolly and the coating top surface were observed each time to assess the failure mode. The fractures, obtained in pull off tests, were mainly adhesive and had tendency to delaminate from the substrate, as shown in Figure 9. The relatively low adhesion of AT13 coatings sprayed by conventional micrometer-sized powders was also reported by other authors [2]. The adhesion of AT13 coatings may still be improved, mainly by the substrate preparation. The abrasive blasting with greater grits is possible in order to increase the substrate roughness prior spraying. Substrate pre-heating may be also considered. Some authors suggest the use of interlayers [32], e.g., nickel-based, to increase the bond-strength of alumina–titania coatings, and this may also be considered in further work.

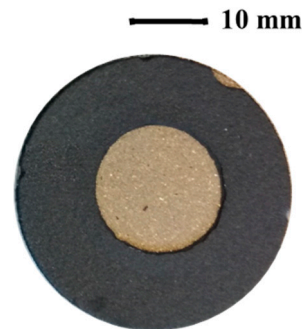


Figure 9. AT13-1 coatings after pull-off tests.

The Vickers microhardness of coatings is presented in Figure 10. The values are influenced by the presence of α - Al_2O_3 , γ - Al_2O_3 , rutile TiO_2 , and Al_2TiO_5 phases. In all coatings, α - Al_2O_3 phase was partially replaced by γ - Al_2O_3 . Vargas et al. [31] reported that those phases in bulk materials are of hardness equal to 1600 and 1400 HV0.1, respectively. The obtained results are lower, due to the presence of Al_2TiO_5 phase, which is of lower hardness [31], as well as the fact that the presence of the following in the coatings—boundaries between lamellas, non-melted particles, porosity, and cracks—can significantly decrease the hardness in comparison to the bulk material. When considering the influence of spray parameters, it can be assumed that the best hardness is provided by the middle torch scan speed and spray distance (coating AT13-3). However, results are quite close to each other. It should also be noticed that coating sprayed from the shorter distance, characterized by better melting of powder particles and more homogeneous structure, show narrower range of standard deviation.

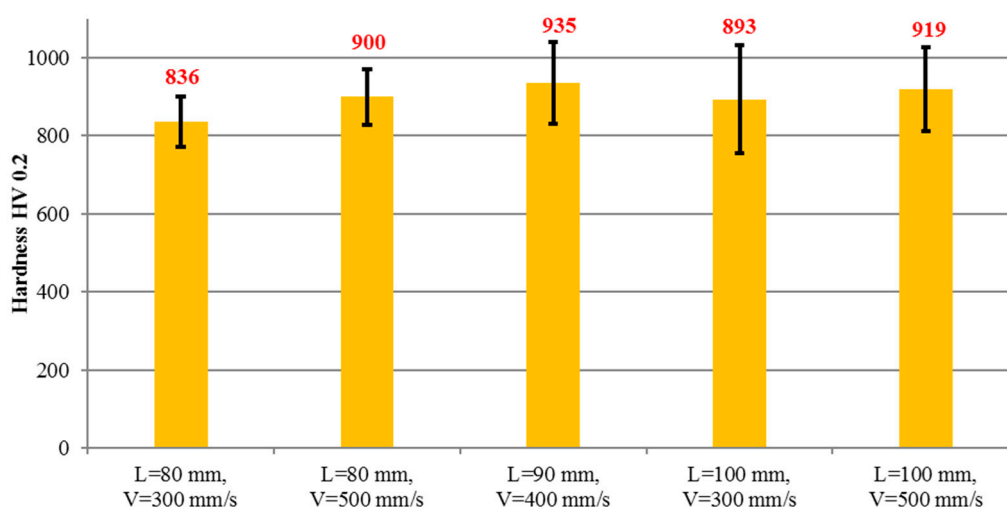


Figure 10. Mean values of coating's microhardness.

The fracture toughness values were calculated by using Anstis approach (Equation (2)). As confirmed by SEM and XRD investigations, non-melted particles were observed in the microstructure of the AT13-5 sample. Additionally, low cohesion between the particles was measured. As a consequence, as cracks propagated easily, low values of fracture toughness were obtained (see Figure 11) [2,40]. Coatings sprayed with the same parameters, but various spray distance (AT13-2) or torch scan speed (AT13-4), so in warmer conditions, were characterized by higher fracture toughness. As reported by H. Luo et al. [18], the effect of bi-modal microstructure may increase the K_{Ic} of $Al_2O_3 + 13 \text{ wt } \% TiO_2$ coatings. This means that the well melted splats and partially melted particles, mixed together in the coating structure, can suppress the crack formation and propagation. However, the obtained results are representative for AT13 APS sprayed coatings. In the literature the fracture toughness of similar deposits is reported to be equal to $3.9 \text{ MPa}\cdot\text{m}^{-1/2}$ [32,41].

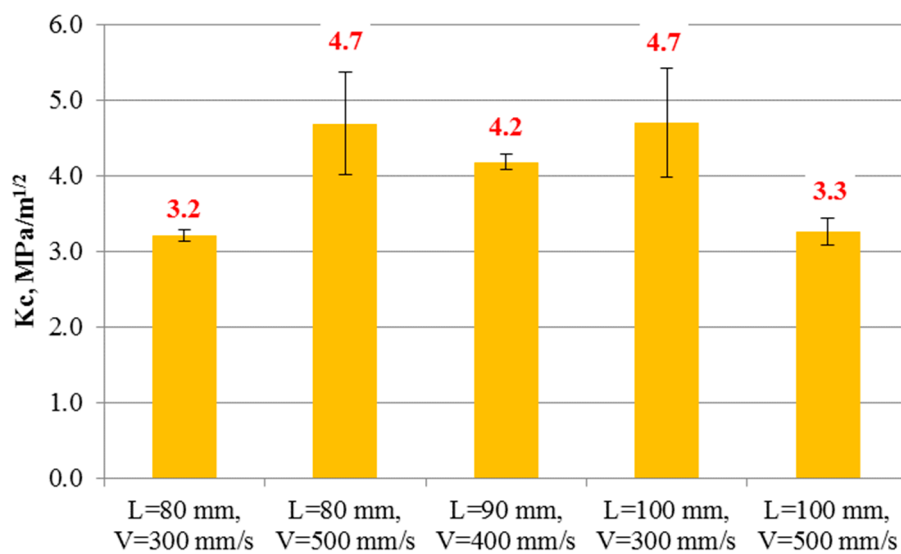


Figure 11. The fracture toughness of AT13 coatings.

Finally, the Ball-on-Disc test allowed to study dry sliding wear resistance of coatings. Coatings dedicated to this investigation were sprayed once again, in order to obtain the similar thickness of $200 \mu\text{m}$, due to the necessity of their grinding and polishing before wear tests. The results are presented in the form of volumetric wear in Figure 12. These results clearly indicate the strong influence of spray process parameters and coating microstructure on the wear resistance. The lowest wear was obtained for AT13-1 and AT13-2 coatings, which were sprayed with the shortest spray distance. The volumetric wear increased with the spray distance and was almost 1.5 times higher for AT13-5 when comparing with AT13-1. It should be pointed out that the high wear resistance was obtained for the coatings with lower content of Al_2TiO_5 .

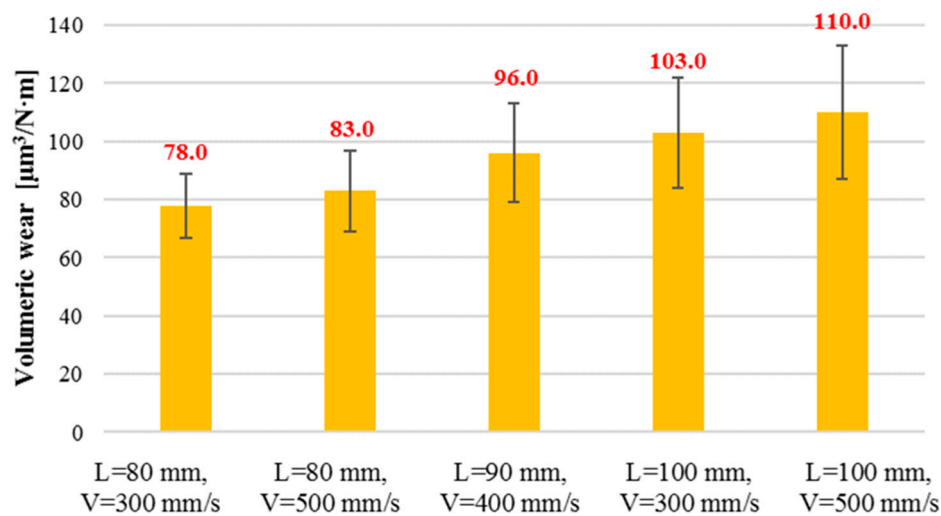


Figure 12. The results of Ball-on-Disc test for AT13 coatings.

The findings can be correlated with SEM observations of wear track surfaces obtained after Ball-on-Disc. As presented in Figure 13, the AT13-1, AT13-3, and AT13-5 coatings showed different behavior when subjected to BoD testing. The wear track of AT13-1 did not reveal significant delamination or damage of coating, which corresponds to relatively low volumetric wear value. It predestines this type of coating for tribological application, for example for covering thread spools. Moreover, this coating is smoother than AT13-5, which contain lots of rough debris. Therefore, the mechanisms based on detachment of loosely bonded particles seemed to be much more dominant in coatings AT13-3 and AT13-5, produced at higher spray distance. These coatings were formed by less-melted particles. This caused much faster removal of material—during counterpart-to-coating contact, the non-fully melted or sintered powder particles were pulled out. This is in agreement with results of, e.g., Vargas et al. [30]. In their study, a strong correlation between fracture toughness and wear resistance was also observed. However, in the presented study, the fracture toughness was influenced by the bi-modal nature of coatings (especially AT13-3 to AT13-5). As discussed earlier, the less-melted regions could inhibit cracking of coating and increase the fracture toughness. But at the same time, the loosely bonded splats were not that resistant to the load applied in Ball-on-Disc testing.

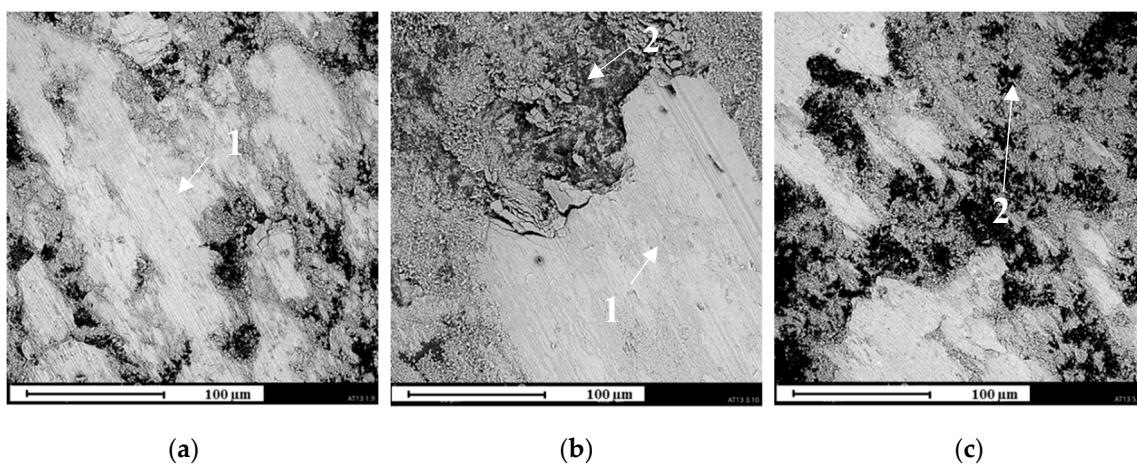


Figure 13. The wear track surface of: (a) AT13-1 (L = 80 mm; V = 300 mm/s), (b) AT13-3 (L = 90 mm; V = 400 mm/s), and (c) AT13-5 coating (L = 100 mm; V = 500 mm/s): 1—smooth wear track, 2—rough debris.

4. Conclusions

In this paper the different spray variables were tested in order to produce $\text{Al}_2\text{O}_3 + 13 \text{ wt } \% \text{TiO}_2$ coatings by atmospheric plasma spraying. The samples were characterized in the terms of their microstructure, phase composition, and various mechanical properties, which are required to provide extended lifetime of the component. The following findings can be summarized:

- Coating microstructure and properties were clearly influenced by the feedstock characteristics. To obtain good coatings, the initial powder properties have to be considered, together with the spraying parameters: the shortest spray distance of 80 mm caused formation of homogeneous coatings with better-melted splats, as the particles impacted the substrate in fully molten state.
- Beside the differences in coatings morphology and microstructure, also observed in the literature, some changes in the phase composition were also noticed. It could also be stated that the ratio of splat area (with $\gamma\text{-Al}_2\text{O}_3$ and anatase- TiO_2) to area with non-melted agglomerates (with $\alpha\text{-Al}_2\text{O}_3$ and rutile- TiO_2) can be controlled by plasma spray parameters. The quantities of the phases depend also on the feedstock material.
- The fracture toughness of coatings depends strongly on the spray parameters. Bi-modal microstructure consisting of well-molten and partially melted particles can provide better resistance (more than 20%) against crack formation than well-melted deposits.
- The homogeneous structure of coating and relatively low porosity (below 7% in each case) allowed obtaining satisfactory results of wear resistance in BoD. The highest volumetric wear was observed for coatings sprayed with the longest spray distance of 100 mm, where microcracking, grooving, and detachment of loosely bonded particles were dominant during wear resistance testing. The shorter spray distance results in around 20% better wear resistance than a longer one. It was established that the spray process parameters have an effect on wear resistance of the coatings.

Further studies will concern mainly the improvement of coating adhesion. The influence of the different TiO_2 additions on the $\text{Al}_2\text{O}_3 + \text{TiO}_2$ coatings produced by APS and SPS is also under investigation.

Author Contributions: Conceptualization L.L. and M.M.; methodology, L.L. and M.M., investigation L.L., M.M. and A.N., resources M.M., writing—original draft preparation M.M., writing—review and editing L.L. and P.S., supervision A.A. All authors have read and agreed to the published version of the manuscript.

Funding: This research received no external funding.

Conflicts of Interest: The authors declare no conflict of interest.

References

1. Sahab, A.R.M.; Saad, N.H.; Kasolang, S.; Saedon, J. Impact of Plasma Spray Variables Parameters on Mechanical and Wear Behaviour of Plasma Sprayed Al_2O_3 3% wt TiO_2 Coating in Abrasion and Erosion Application. *Procedia Eng.* **2012**, *41*, 1689–1695. [[CrossRef](#)]
2. Vicent, M.; Bannier, E.; Benavente, R.; Salvador, M.D.; Molina, T.; Moreno, R.; Sánchez, E. Influence of the feedstock characteristics on the microstructure and properties of $\text{Al}_2\text{O}_3\text{-TiO}_2$ plasma-sprayed coatings. *Surf. Coat. Technol.* **2013**, *220*, 74–79. [[CrossRef](#)]
3. Geaman, V.; Pop, M.A.; Motoc, D.L.; Radomir, I. Tribological properties of thermal spray coatings. *Eur. Sci. J. ESJ* **2014**, *3*, 154–159.
4. Singh, V.P.; Sil, A.; Jayaganthan, R. Tribological behavior of plasma sprayed $\text{Cr}_2\text{O}_3\text{-3%TiO}_2$ coatings—ScienceDirect. *Wear* **2011**, *272*, 149–158. [[CrossRef](#)]
5. Steeper, T.J.; Varacalle, D.J.; Wilson, G.C.; Riggs, W.L.; Rotolico, A.J.; Nerz, J. A design of experiment study of plasma-sprayed alumina-titania coatings. *J. Therm. Spray Technol.* **1993**, *2*, 251–256. [[CrossRef](#)]
6. Toma, F.-L.; Berger, L.-M.; Stahr, C.C.; Naumann, T.; Langner, S. Microstructures and Functional Properties of Suspension-Sprayed Al_2O_3 and TiO_2 Coatings: An Overview. *J. Therm. Spray Technol.* **2010**, *19*, 262–274. [[CrossRef](#)]

7. Szala, M.; Walczak, M.; Pasierbiewicz, K.; Kamiński, M. Cavitation Erosion and Sliding Wear Mechanisms of AlTiN and TiAlN Films Deposited on Stainless Steel Substrate. *Coatings* **2019**, *9*, 340. [[CrossRef](#)]
8. Matikainen, V.; Niemi, K.; Koivuluoto, H.; Vuoristo, P. Abrasion, Erosion and Cavitation Erosion Wear Properties of Thermally Sprayed Alumina Based Coatings. *Coatings* **2014**, *4*, 18–36. [[CrossRef](#)]
9. Stengl, V.; Ageorges, H.; Ctibor, P.; Murafa, N. Atmospheric plasma sprayed (APS) coatings of Al₂O₃-TiO₂ system for photocatalytic application. *Photochem. Photobiol. Sci.* **2009**, *8*, 733–738. [[CrossRef](#)]
10. Tomaszek, R.; Pawlowski, L.; Zdanowski, J.; Grimblot, J.; Laurey, J. Microstructural transformations of TiO₂, Al₂O₃+13TiO₂ and Al₂O₃+40TiO₂ at plasma spraying and laser engraving. *Surf. Coat. Technol.* **2004**, *185*, 137–149. [[CrossRef](#)]
11. Żórawski, W.; Góral, A.; Bokuvka, O.; Lityńska-Dobrzyńska, L.; Berent, K. Microstructure and tribological properties of nanostructured and conventional plasma sprayed alumina-titania coatings. *Surf. Coat. Technol.* **2015**, *268*, 190–197. [[CrossRef](#)]
12. Ibrahim, A.; Hamdy, A.S. Microstructure, Corrosion, and Fatigue Properties of Alumina-Titania Nanostructured Coatings. *J. Surf. Eng. Mater. Adv. Technol.* **2011**, *1*, 101. [[CrossRef](#)]
13. Ghazali, M.J.; Forghani, S.M.; Hassanuddin, N.; Muchtar, A.; Daud, A.R. Comparative wear study of plasma sprayed TiO₂ and Al₂O₃-TiO₂ on mild steels—ScienceDirect. *Tribol. Int.* **2016**, *93*, 681–686. [[CrossRef](#)]
14. Richter, A.; Berger, L.-M.; Conze, S.; Sohn, Y.J.; Vassen, R. Emergence and impact of Al₂TiO₅ in Al₂O₃-TiO₂ APS coatings. *Mater. Sci. Eng.* **2019**, *480*, 012007. [[CrossRef](#)]
15. Goberman, D.; Sohn, Y.H.; Shaw, L.; Jordan, E.; Gell, M. Microstructure development of Al₂O₃-13 wt % TiO₂ plasma sprayed coatings derived from nanocrystalline powders. *Acta Mater.* **2002**, *50*, 1141–1152. [[CrossRef](#)]
16. Góral, A.; Żórawski, W.; Lityńska-Dobrzyńska, L. Study of the microstructure of plasma sprayed coatings obtained from Al₂O₃-13TiO₂ nanostructured and conventional powders. *Mater. Charact.* **2014**, *96*, 234–240. [[CrossRef](#)]
17. Jordan, E.H.; Gell, M.; Sohn, Y.H.; Goberman, D.; Shaw, L.; Jiang, S.; Wang, M.; Xiao, T.D.; Wang, Y.; Strutt, P. Fabrication and evaluation of plasma sprayed nanostructured alumina-titania coatings with superior properties. *Mater. Sci. Eng. A* **2001**, *301*, 80–89. [[CrossRef](#)]
18. Luo, H.; Goberman, D.; Shaw, L.; Gell, M. Indentation fracture behavior of plasma-sprayed nanostructured Al₂O₃-13 wt.%TiO₂ coatings. *Mater. Sci. Eng. A* **2003**, *346*, 237–245. [[CrossRef](#)]
19. Pawłowski, L. *The Science and Engineering of Thermal Spray Coatings*, 2nd ed.; Wiley: Chichester, UK, 2008; ISBN 978-0-471-49049-4.
20. Fauchais, P.L.; Heberlein, J.V.R.; Boulos, M. *Thermal Spray Fundamentals: From Powder to Part*; Springer: New York, NY, USA, 2014; ISBN 978-0-387-28319-7.
21. Wahab, J.A.; Ghazali, M.J.; Baharin, A.F.S. Microstructure and mechanical properties of plasma sprayed Al₂O₃-13%TiO₂ Ceramic Coating. *MATEC Web Conf.* **2017**, *87*, 02027. [[CrossRef](#)]
22. Pawlowski, L. Suspension and solution thermal spray coatings. *Surf. Coat. Technol.* **2009**, *203*, 2807–2829. [[CrossRef](#)]
23. ASTM E2109-01 01 Standard Test Methods for Determining Area Percentage Porosity in Thermal Sprayed Coatings; ASTM: West Conshohocken, PA, USA, 2014.
24. EN ISO 4516: 2004 Metallic and other Inorganic Coatings—Vickers and Knoop Microhardness Tests; Swiss Association for Standardization: Winterthur, Switzerland, 2004.
25. Palmqvist, S. Occurrence of crack formation during Vickers indentation as a measure of the toughness of hard materials. *Arch. Eisenhuettenwes* **1962**, *33*, 629–634.
26. Niihara, K. A fracture mechanics analysis of indentation-induced Palmqvist crack in ceramics. *J. Mater. Sci. Lett.* **1983**, *2*, 221–223. [[CrossRef](#)]
27. Chantikul, P.; Anstis, G.R.; Lawn, B.R.; Marshall, D.B. A Critical Evaluation of Indentation Techniques for Measuring Fracture Toughness: II, Strength Method. *J. Am. Ceram. Soc.* **1981**, *64*, 539–543. [[CrossRef](#)]
28. Pędzich, Z.; Piekarczyk, J.; Stobierski, L.; Szutkowska, M.; Walat, E. Twadość Vickersa i odporność na pękanie wybranych kompozytów ceramicznych. *Kompozyty* **2003**, *3*, 296–300.
29. Michalak, M.; Łatka, L.; Sokołowski, P. Comparison of mechanical properties of the plasma sprayed coatings by powder and suspension. *Weld. Technol. Rev.* **2017**, *89*, 56–60.
30. ASTM G99-17 Standard Test Method for Wear Testing with a Pin-on-Disk Apparatus; ASTM: West Conshohocken, PA, USA, 2016.

31. Vargas, F.; Ageorges, H.; Fournier, P.; Fauchais, P.; Lopez, M.E. Mechanical and tribological performance of Al₂O₃-TiO₂ coatings elaborated by flame and plasma spraying - ScienceDirect. *Surf. Coat. Technol.* **2010**, *205*, 1132–1136. [[CrossRef](#)]
32. Yılmaz, Ş. An evaluation of plasma-sprayed coatings based on Al₂O₃ and Al₂O₃-13wt.% TiO₂ with bond coat on pure titanium substrate. *Ceram. Int.* **2009**, *35*, 2017–2022. [[CrossRef](#)]
33. Yao, S.H.; Su, Y.L.; Shu, H.Y.; Lee, C.I.; You, Z.L. Comparative Study on Nano-Structural and Traditional Al₂O₃-13TiO₂ Air Plasma Sprayed Coatings and their Thermal Shock Performance. *Key Eng. Mater.* **2017**, *739*, 103–107. [[CrossRef](#)]
34. Czanderna, A.W.; Rao, C.N.R.; Honig, J.M. The anatase-rutile transition. Part 1—Kinetics of the transformation of pure anatase. *Trans. Faraday Soc.* **1958**, *54*, 1069–1073. [[CrossRef](#)]
35. Dachille, F.; Simons, P.Y.; Roy, R. Pressure-temperature studies of anatase, brookite, rutile and TiO₂-II. *Am. Mineral.* **1968**, *53*, 1929–1939.
36. Shaw, L.L.; Goberman, D.; Ren, R.; Gell, M.; Jiang, S.; Wang, Y.; Xiao, T.D.; Strutt, P.R. The dependency of microstructure and properties of nanostructured coatings on plasma spray conditions. *Surf. Coat. Technol.* **2000**, *130*, 1–8. [[CrossRef](#)]
37. Berger, L.-M.; Toma, F.-L.; Scheitz, S.; Trache, R.; Börner, T. Thermisch gespritzte Schichten im System Al₂O₃-Cr₂O₃-TiO₂—Ein Update. *Mater. Werkst.* **2014**, *45*, 465–475. [[CrossRef](#)]
38. Freudenberg, F. Etude de la réaction à l'état solide Al₂O₃ + TiO₂ → Al₂TiO₅: Observation des structures: Thèse VÉ cole polytechnique fédérale de Lausanne EPFL. *EPFL Lausanne* **1988**, 709.
39. Berger, L.-M. Tribology of thermally sprayed coatings in the Al₂O₃-Cr₂O₃-TiO₂ system. In *Thermal Sprayed Coatings and Their Tribological Performances*; Engineering Science Reference; IGI Global: Hershey, PA, USA, 2015; pp. 227–267. ISBN 978-1-4666-7489-9.
40. Łatka, L.; Niemiec, A.; Michalak, M.; Sokołowski, P. Tribological properties of Al₂O₃+ TiO₂ coatings manufactured by plasma spraying. *Tribology* **2019**, *1*, 19–24. [[CrossRef](#)]
41. Dejang, N.; Watcharapasorn, A.; Wirojupatump, S.; Niranatlumpong, P.; Jiansirisomboon, S. Fabrication and properties of plasma-sprayed Al₂O₃/TiO₂ composite coatings: A role of nano-sized TiO₂ addition. *Surf. Coat. Technol.* **2010**, *204*, 1651–1657. [[CrossRef](#)]



© 2020 by the authors. Licensee MDPI, Basel, Switzerland. This article is an open access article distributed under the terms and conditions of the Creative Commons Attribution (CC BY) license (<http://creativecommons.org/licenses/by/4.0/>).